



MODAL VIBRATION DAMPING OF ANISOTROPIC FRP LAMINATES USING THE RAYLEIGH–RITZ ENERGY MINIMIZATION SCHEME

M. R. MAHERI AND R. D. ADAMS

Department of Mechanical Engineering, University of Bristol, Queens Building, University Walk, Bristol BS8 1TR, England. E-mail: r.d.adams@bristol.ac.uk

(Received 4 September 2001, and in final form 5 February 2002)

The Rayleigh–Ritz method has been used for computing the modal damping of structural orthotropic materials, including anisotropic laminates, in free vibration. Comparison of the theoretical results has been made with experimental data obtained from tests on freely held plates, and with the results obtained from the finite element method. It has been shown that the Rayleigh–Ritz scheme can be used to predict accurately the modal damping of thin rectangular plates, and that its prediction of modal characteristics of such plates correlates closely with that of the finite element method.

© 2002 Elsevier Science Ltd. All rights reserved.

1. INTRODUCTION

One of the advantages of using fibre-reinforced plastic (FRP) composites in weight-sensitive applications is their inherent damping capacity which, compared to metals, is structurally useful. It is also well known that laminated FRP panels show considerable variation in their damping capacity in different modes of vibration, owing to the anisotropic nature of their elastic and damping properties, and the elastic and damping properties are themselves affected by a number of variables including the laminae fibre orientation and stacking sequence. Although manipulation of the inherent damping capacity of the material may often not be a primary design objective, there is, nevertheless, little reason as to why the modal damping capacities cannot be readily estimated, at least for qualitative design purposes.

There have been two main approaches to damping analyses. One is based on the concept of material damping which arises from the stress–strain hysteretic losses and is independent of strain rate, and one that is based on the linear viscoelasticity theory and is a function of strain rate [1, 2]. These are both idealized “linear” damping models which are limited in their scope. However, the material damping model is more suited to relatively low-damping structural materials at levels of cyclic stress below the fatigue limit, while the viscoelastic damping model is more suited to the highly damped viscoelastic materials usually sandwiched between elastic layers in added damping treatment. The hysteretic material damping mechanism has often been the preferred model for damping analysis of FRP composites under normal working conditions. This is partly because it is an easier model to use for damping analyses, but also because the thermosetting resins that are used in FRP composite laminates are relatively hard materials with low damping which show little frequency dependence except at temperatures near the glass transition temperature.

An early hypothesis of the damping mechanism in orthotropic FRP laminae was proposed by Adams and Bacon [3] in which the damping energy was assumed to be the sum of separable energy dissipations due to principal stress components in the lamina fibre co-ordinate system, including stresses along and across the fibres and the in-plane longitudinal shear stress. This simple model was effective in computing the modal damping of laminated composite beams and plates [4–10]. Using essentially the same assumed damping mechanism, Saravanos and Chamis [11] have presented a methodology for optimizing the damping in laminated composite beams and shells subject to forced vibration in terms of fibre orientation as well as fibre volume fraction. In a later work [12], variation of the modal characteristics of laminated plates with added interlaminar damping layers was considered as a function of such design variables as damping layer thickness, plate aspect ratio and fibre volume fraction.

Unless the plate is simply supported and is free from any coupling between bending and stretching and bending and twisting (“specially orthotropic”), for which case exact solutions exist [13], modal characteristics of laminated plates are normally obtained by numerical approximation methods such as that of Rayleigh–Ritz, or the more generalized finite element (FE) method. The latter method has been used by various authors [5, 9] to compute the modal damping of laminated plates, and good correlation with experimental values have been reported. However, the Rayleigh–Ritz method involves considerably less computation than the FE method, and it would be advantageous on that account alone to use this method where possible [14, 15]. It is the aim of the present work to use the Rayleigh–Ritz method to compute the modal damping of anisotropic-laminated plates, and to compare the theoretical results with values obtained experimentally, and with those obtained by the FE method. The transverse shear effects have not been considered in the present work, although these become of increased significance in thicker laminates and at higher frequencies and modal densities than considered here.

2. THEORY

2.1. DAMPING IN LAMINATED FRP MATERIALS

The specific damping capacity (SDC) is used as the measure of damping in this work. It is defined as the ratio Ψ of the damping energy ΔU dissipated per cycle of vibration, to the maximum strain energy, U such that

$$\Psi = \frac{\Delta U}{U}. \quad (1)$$

In the fibre co-ordinate system (Figure 1), the strain energy in a uni-directional lamina under a state of plane stress is given by

$$U = \frac{1}{2} \int_v \{\boldsymbol{\sigma}_i\}^T \{\boldsymbol{\varepsilon}_i\} dv \quad (i = 1, 2, 6), \quad (2)$$

where

$$\{\boldsymbol{\sigma}_i\} = [\mathbf{Q}_{ij}] \{\boldsymbol{\varepsilon}_j\} \quad (i, j = 1, 2, 6) \quad (3)$$

and $[\mathbf{Q}_{ij}]$ is the on-axis reduced plane stress stiffness matrix. $[\mathbf{Q}_{ij}]$ is a symmetric matrix whose elements are given in terms of four independent, orthotropic, elastic properties, including the in-plane moduli E_1 , E_2 , the longitudinal shear modulus G_{12} and the major

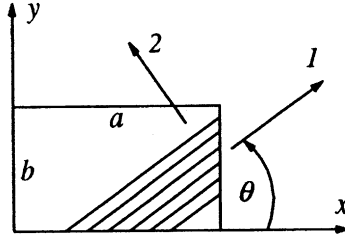


Figure 1. Plate co-ordinates and lamina orientation.

Poisson's ratio ν_{12} :

$$\begin{aligned} Q_{11} &= \frac{E_1^2}{(E_1 - \nu_{12}^2 E_2)}, & Q_{12} &= \frac{\nu_{12} E_1 E_2}{(E_1 - \nu_{12}^2 E_2)}, & Q_{22} &= \frac{E_1 E_2}{(E_1 - \nu_{12}^2 E_2)}, \\ Q_{66} &= G_{12}, & \text{and } Q_{16} &= Q_{26} = 0. \end{aligned} \quad (4)$$

Assuming that the damping energy is the sum of separable energy dissipations due to stress components [3], then the total dissipated energy is similarly given by

$$\Delta U = \frac{1}{2} \int_v \{\boldsymbol{\sigma}_i\}^T [\boldsymbol{\Psi}] \{\boldsymbol{\varepsilon}_i\} dv, \quad (5)$$

in which the damping matrix $[\boldsymbol{\Psi}]$ is the diagonal matrix

$$[\boldsymbol{\Psi}] = \begin{bmatrix} \psi_1 & & \mathbf{0} \\ & \psi_2 & \\ \mathbf{0} & & \psi_6 \end{bmatrix}, \quad (6)$$

where the factors ψ_i quantify the proportion of the energy loss in each cycle of vibration due to each stress component.

In mid-plane symmetric laminates, the bending and stretching are decoupled, and when such a laminate is subjected to bending only, the strains $\{\boldsymbol{\varepsilon}_i\}$ at a distance z from the neutral axis can be found in terms of the curvatures $\{\boldsymbol{\chi}_i\}$

$$\{\boldsymbol{\varepsilon}_i\} = z\{\boldsymbol{\chi}_i\}. \quad (7)$$

Substituting for $\{\boldsymbol{\varepsilon}_i\}$ from equation (7), and for $\{\boldsymbol{\sigma}_i\}$ from equation (3) into equation (2) gives

$$U = \frac{1}{2} \int_v \{\boldsymbol{\chi}_i\}^T [\mathbf{Q}_{ij}] \{\boldsymbol{\chi}_i\} z^2 dv. \quad (8)$$

Using the strain transformation relationship,

$$\{\boldsymbol{\varepsilon}_i\} = [\mathbf{T}] \{\boldsymbol{\varepsilon}_{x,y}\} \quad (9)$$

in which

$$[\mathbf{T}] = \begin{bmatrix} m^2 & n^2 & mn \\ n^2 & m^2 & -mn \\ -2mn & 2mn & m^2 - n^2 \end{bmatrix}, \quad \text{where } m = \cos(\theta) \text{ and } n = \sin(\theta),$$

then the strain energy takes the following form with respect to the laminate co-ordinate system (x, y) shown in Figure 1:

$$U = \frac{1}{2} \int_v ([\mathbf{T}] \{\boldsymbol{\chi}_{x,y}\})^T [\mathbf{Q}_{ij}] [\mathbf{T}] \{\boldsymbol{\chi}_{x,y}\} z^2 dv = \frac{1}{2} \int_v \{\boldsymbol{\chi}_{x,y}\}^T [\bar{\mathbf{Q}}_{ij}] \{\boldsymbol{\chi}_{x,y}\} z^2 dv \quad (10)$$

in which

$$[\bar{\mathbf{Q}}_{ij}] = [\mathbf{T}]^T [\mathbf{Q}_{ij}] [\mathbf{T}] \quad (11)$$

is the reduced off-axis plane stress stiffness matrix. The curvatures $\{\chi_{x,y}\}$ are given as

$$\{\chi_{x,y}\} = \begin{Bmatrix} \chi_x \\ \chi_y \\ \chi_{xy} \end{Bmatrix} = - \begin{Bmatrix} \frac{\partial^2 w}{\partial x^2} \\ \frac{\partial^2 w}{\partial y^2} \\ 2 \frac{\partial^2 w}{\partial x \partial y} \end{Bmatrix}, \quad (12)$$

where w is the lateral deflection. Since the curvatures are invariant of z , equation (10) can be simplified by integrating through the thickness h of the laminate over $[\bar{\mathbf{Q}}_{ij}]$, namely

$$U = \frac{1}{2} \int_{\Omega} \{\chi_{x,y}\}^T \left(\int_{-h/2}^{h/2} [\bar{\mathbf{Q}}_{ij}] z^2 dz \right) \{\chi_{x,y}\} d\Omega = \frac{1}{2} \int_{\Omega} \{\chi_{x,y}\}^T [\mathbf{D}_{ij}] \{\chi_{x,y}\} d\Omega, \quad (13)$$

where Ω is the area of the plate and

$$[\mathbf{D}_{ij}] = \int_{-h/2}^{h/2} [\bar{\mathbf{Q}}_{ij}] z^2 dz = \frac{2}{3} \sum_{k=1}^{L/2} [\bar{\mathbf{Q}}_{ij}^k] (h_k^3 - h_{(k-1)}^3), \quad (14)$$

in which h_k and $h_{(k-1)}$ are the upper and lower ordinates of the k th lamina, respectively, and L is the total number of laminae. When the latter are all of the same material and thickness, then this expression is further simplified to

$$[\mathbf{D}_{ij}] = \frac{2}{3} \left(\frac{h}{L} \right)^3 \sum_{k=1}^{L/2} [\bar{\mathbf{Q}}_{ij}^k] (k^3 - (k-1)^3), \quad (15)$$

where $[\mathbf{D}_{ij}]$ is the bending stiffness matrix of the laminate and, like $[\bar{\mathbf{Q}}_{ij}]$, is fully populated and symmetric. Substituting for curvatures from equation (12) into equation (13), and expanding the resulting expression gives

$$U = \frac{1}{2} \int_0^a \int_0^b \left\{ D_{11} \left(\frac{\partial^2 w}{\partial x^2} \right)^2 + 2D_{12} \frac{\partial^2 w}{\partial x^2} \frac{\partial^2 w}{\partial y^2} + D_{22} \left(\frac{\partial^2 w}{\partial y^2} \right)^2 + 4D_{16} \frac{\partial^2 w}{\partial x^2} \frac{\partial^2 w}{\partial x \partial y} + 4D_{26} \frac{\partial^2 w}{\partial y^2} \frac{\partial^2 w}{\partial x \partial y} + 4D_{66} \left(\frac{\partial^2 w}{\partial x \partial y} \right)^2 \right\} dx dy. \quad (16)$$

The expression for ΔU (equation (5)) can be developed in a similar fashion to that for developing U , and it will be seen that, in analogy with equation (10), the following expression results for the damping energy:

$$\Delta U = \frac{1}{2} \int_v \{\chi_{x,y}\}^T [\mathbf{T}]^T [\boldsymbol{\Psi}] [\mathbf{Q}_{ij}] [\mathbf{T}] \{\chi_{x,y}\} z^2 dv = \frac{1}{2} \int_v \{\chi_{x,y}\}^T [\mathbf{R}_{ij}] \{\chi_{x,y}\} z^2 dv, \quad (17)$$

in which the ‘‘damped stiffness matrix’’

$$[\mathbf{R}_{ij}] = [\mathbf{T}]^T [\boldsymbol{\Psi}] [\mathbf{Q}_{ij}] [\mathbf{T}] \quad (18)$$

is generally non-symmetric. Integrating through the thickness over $[\mathbf{R}_{ij}]$, the damping energy becomes

$$\Delta U = \frac{1}{2} \int_{\Omega} \{\chi_{x,y}\}^T [\mathbf{d}_{ij}] \{\chi_{x,y}\} d\Omega, \quad (19)$$

in which the damped bending stiffness matrix is given as

$$[\mathbf{d}_{ij}] = \frac{2}{3} \left(\frac{h}{L} \right)^3 \sum_{k=1}^{L/2} [\mathbf{R}_{ij}^k] (k^3 - (k-1)^3). \quad (20)$$

Substituting for curvatures from equation (12) into equation (19), and expanding gives

$$\begin{aligned} \Delta U = \frac{1}{2} \int_0^a \int_0^b \left\{ d_{11} \left(\frac{\partial^2 w}{\partial x^2} \right)^2 + (d_{12} + d_{21}) \frac{\partial^2 w}{\partial x^2} \frac{\partial^2 w}{\partial y^2} + d_{22} \left(\frac{\partial^2 w}{\partial y^2} \right)^2 \right. \\ \left. + 2(d_{16} + d_{61}) \frac{\partial^2 w}{\partial x^2} \frac{\partial^2 w}{\partial x \partial y} + 2(d_{26} + d_{62}) \frac{\partial^2 w}{\partial y^2} \frac{\partial^2 w}{\partial x \partial y} + 4d_{66} \left(\frac{\partial^2 w}{\partial x \partial y} \right)^2 \right\} dx dy. \quad (21) \end{aligned}$$

Strictly speaking, the factors ψ_i in equation (6) are functions of the stress amplitude within the material. However, in the idealized *linear damping* mechanism, which can be expected to be nearer realization at lower stress amplitudes, these factors can be assumed to be independent of the stress amplitude. In that case, the shape of the hysteretic loop becomes elliptical [1, 2], and ψ_i become constant material properties. The orthotropic elastic and damping properties can be measured from tests on uni-directional beam specimens with 0 and 90° fibre orientation [4, 8] (reference [15] gives an alternative method for determining the elastic properties from modal tests on orthotropic plates).

2.2. MODAL CHARACTERISTICS BY THE RAYLEIGH–RITZ METHOD

The Rayleigh–Ritz method is covered extensively in the literature. A detailed account of the method for isotropic plates has been given by Young [16], and that for anisotropic-laminated plates by Ashton and Waddoups [14] and Ashton and Whitney [13]. An outline of the application of the Rayleigh–Ritz method to modal vibration of anisotropic-laminated plates, together with its utilization in computing the modal damping of such plates, is given here.

The method involves expressing the lateral deflection of a rectangular plate in terms of a summation of a series of the products of two one-dimensional functions in the x and y directions with unknown coefficients, thus

$$w = \sum_{m=1}^M \sum_{n=1}^N A_{mn} X_m(x) Y_n(y). \quad (22)$$

The functions $X_m(x)$ and $Y_n(y)$ should be differentiable, at least to the order of derivatives appearing in the energy expressions, and they should conform to, at least, the geometric boundary conditions of the problem. Bernoulli–Euler-type beam functions [16] have been a popular choice for these functions, although improvement in the results have been reported by using Timoshenko beam equations (for Mindlin plates) [17, 18], orthogonal polynomials [19] and plate functions [20]. Minimizing the total energy of the system with respect to the coefficients would form the eigenvalue problem, the solution of which would yield the frequencies and the unknown coefficients.

Since, the total energy of the system is constant at any given time, the following holds:

$$U - T = \text{constant}, \quad (23)$$

in which for a uniform plate, the kinetic energy of the normal mode of vibration is given by

$$T = \frac{1}{2} \rho \omega^2 h \int_0^a \int_0^b w^2 dx dy, \quad (24)$$

where ρ is the density of the plate, and ω is the circular frequency of the normal mode.

Substituting for w and its derivatives from equation (22) into equations (16) and (24), and substituting the resulting expressions for U and T into equation (23), and rearranging the latter expression, so that the functions of x and y are separated into their respective integration domains then, on minimizing the total energy with respect to the coefficients A_{ij} , one obtains the following expression:

$$\begin{aligned} \frac{\partial}{\partial A_{ij}}(U - T) = & \sum_{i=1}^M \sum_{j=1}^N \left\{ D_{11} \int_0^a X_i'' X_m'' dx \int_0^b Y_j Y_n dy + D_{22} \int_0^a X_i X_m dx \int_0^b Y_j'' Y_n'' dy \right. \\ & + D_{12} \left[\int_0^a X_m X_i'' dx \int_0^b Y_j Y_n'' dy + \int_0^a X_i X_m'' dx \int_0^b Y_n Y_j'' dy \right] \\ & + 2D_{16} \left[\int_0^a X_i'' X_m' dx \int_0^b Y_j Y_n' dy + \int_0^a X_i' X_m'' dx \int_0^b Y_n Y_j' dy \right] \\ & + 2D_{26} \left[\int_0^a X_m X_i' dx \int_0^b Y_j' Y_n'' dy + \int_0^a X_i X_m' dx \int_0^b Y_j'' Y_n' dy \right] \\ & \left. + 4D_{66} \int_0^a X_i' X_m' dx \int_0^b Y_j' Y_n' dy - \rho \omega^2 h \int_0^a X_i X_m dx \int_0^b Y_j Y_n dy \right\} A_{mn} = 0 \\ & (m = 1, 2, \dots, M; n = 1, 2, \dots, N), \end{aligned} \quad (25)$$

in which the number of primes indicates the order of the derivative of the function with respect to its argument. Following the work of Young [16] and Ashton and Waddoups [14] in using Bernoulli–Euler-type beam functions with free and/or clamped end conditions, the functions $X_{(i,m)}(x)$ and $Y_{(j,n)}(y)$ can be conveniently represented in the following general form:

$$\varphi_s(r) = \cosh \frac{\lambda_s r}{l} + F_1 \cos \frac{\lambda_s r}{l} + \gamma_s \left(-\sinh \frac{\lambda_s r}{l} + F_2 \sin \frac{\lambda_s r}{l} \right), \quad (26)$$

in which l is the length of the beam, and $F_1 = +1$, $F_2 = -1$ for a free–free beam, $F_1 = -1$, $F_2 = +1$ for a clamped–clamped and a clamped–free beam, and λ_s is the s th root of the beam characteristic equation. The latter is, similarly, presented here in the following general form:

$$\cos \lambda_s \cosh \lambda_s + F_3 = 0, \quad (27)$$

in which, $F_3 = -1$ for a free–free and for a clamped–clamped beam, and $F_3 = +1$ for a clamped–free beam. Finally, the factor γ_s in equation (26) is given by

$$\gamma_s = \frac{(\cosh \lambda_s + F_4 \cos \lambda_s)}{(\sinh \lambda_s + F_4 \sin \lambda_s)}, \quad (28)$$

in which, $F_4 = -1$ for a free–free and for a clamped–clamped beam, and $F_4 = +1$ for a clamped–free beam. It is noted that for a free–free beam, the first two modes are rigid-body motion modes given by

$$\varphi_1(r) = 1 \quad \text{and} \quad \varphi_2(r) = \sqrt{3}(1 - 2r/l). \quad (29)$$

If, therefore, it is required to analyze a plate which has, for example, one side along the x direction (Figure 1) clamped and the remaining sides free, then the function $X(x)$ would be the free-free beam function and $Y(y)$ the clamped-free beam function. For a plate with all edges free, both functions would be free-free beam functions, and so on. Generally, however, the (natural) boundary conditions of a free edge in a plate are not completely satisfied by the use of the corresponding free-end beam functions. Nevertheless, experimental evidence tends to suggest that this has only a marginal effect on the results [14, 17].

Equation (25) can be written in the matrix form

$$([\mathbf{K}_{kl}] - \omega^2[\mathbf{M}_{kl}])\{\mathbf{A}_l\} = \mathbf{0} \quad (30)$$

such that $k = (i - 1)N + j$ and $l = (m - 1)N + n$. The matrices $[\mathbf{K}]$ and $[\mathbf{M}]$ so assembled correspond to the stiffness and mass matrix, respectively, and $\{\mathbf{A}\}$ is the vector of the unknown coefficients. Equation (30) can be rearranged into the generalized eigenproblem form

$$\mathbf{K}\mathbf{A} = \omega^2\mathbf{M}\mathbf{A}. \quad (31)$$

On pre-multiplying this equation by \mathbf{K}^{-1} , and rearranging to give

$$\mathbf{K}^{-1}\mathbf{M}\mathbf{A} = \Lambda\mathbf{A}, \quad (32)$$

in which $\Lambda = 1/\omega^2$, then the solution of equation (32) by an iterative method will yield the modal characteristics ω , \mathbf{A} of the more prominent, lower modes first. In the present case of free-free plates, where \mathbf{K} was singular owing to the presence of rigid-body modes, a spectrum shift technique [21] was used to overcome the problem.

To compute the modal specific damping capacity, the strain energy U and the damping energy ΔU are obtained by substituting for w from equation (22) into equations (16) and (21) respectively.

$$\begin{aligned} U = & \frac{1}{2} \sum_{i=1}^M \sum_{j=1}^N A_{ij} \left\{ D_{11} \int_0^a X_i'' X_m'' dx \int_0^b Y_j Y_n dy + 2D_{12} \int_0^a X_i'' X_m dx \int_0^b Y_j Y_n'' dy \right. \\ & + D_{22} \int_0^a X_i X_m dx \int_0^b Y_j'' Y_n'' dy + 4D_{16} \int_0^a X_i'' X_m' dx \int_0^b Y_j Y_n' dy \\ & \left. + 4D_{26} \int_0^a X_i X_m' dx \int_0^b Y_j'' Y_n' dy + 4D_{66} \int_0^a X_i' X_m' dx \int_0^b Y_j' Y_n' dy \right\} A_{mn} \\ & (m = 1, 2, \dots, M; n = 1, 2, \dots, N), \end{aligned} \quad (33)$$

$$\begin{aligned} \Delta U = & \frac{1}{2} \sum_{i=1}^M \sum_{j=1}^N A_{ij} \left\{ d_{11} \int_0^a X_i'' X_m'' dx \int_0^b Y_j Y_n dy + (d_{12} + d_{21}) \int_0^a X_i'' X_m dx \int_0^b Y_j Y_n'' dy \right. \\ & + d_{22} \int_0^a X_i X_m dx \int_0^b Y_j'' Y_n'' dy + 2(d_{16} + d_{61}) \int_0^a X_i'' X_m' dx \int_0^b Y_j Y_n' dy \\ & \left. + 2(d_{26} + d_{62}) \int_0^a X_i X_m' dx \int_0^b Y_j'' Y_n' dy + 4d_{66} \int_0^a X_i' X_m' dx \int_0^b Y_j' Y_n' dy \right\} A_{mn} \\ & (m = 1, 2, \dots, M; n = 1, 2, \dots, N), \end{aligned} \quad (34)$$

where the latter expression is exactly the same as the former, but with different multipliers in its terms.

For any generalized modal displacements $\{\mathbf{A}\}$ obtained from the solution of the eigenproblem, the specific damping capacity of the plate in that particular mode can be

computed from equations (1), (33) and (34), and the nodal pattern can be obtained from equation (22). Since the maximum values of the strain and kinetic energies are the same (neglecting the damping energy), it might be more convenient to use the more simple expression for the kinetic energy in place of the one for the strain energy (equation (33)) for computation of the SDC. The kinetic energy is obtained by substituting for w from equation (22) into equation (24) to give

$$T = \frac{1}{2} \rho \omega^2 h \left[\sum_{i=1}^M \sum_{j=1}^N A_{ij} \int_0^a X_i X_m dx \int_0^b Y_j Y_n dy \right] A_{mm} \quad (m = 1, 2, \dots, M; \quad n = 1, 2, \dots, N). \quad (35)$$

It is noted that some of the integrals in equation (25) and the energy expressions (33)–(35) can be simplified by making use of the following properties of the orthogonality of normal modes as applied to lateral vibration of Bernoulli–Euler beams:

$$\varphi_p(r) \varphi_q(r) = \begin{cases} 1 & \text{for } p = q \\ 0 & \text{for } p \neq q \end{cases} \quad \text{and} \quad \varphi_p''(r) \varphi_q''(r) = \begin{cases} (\lambda_p/l)^4 & \text{for } p = q \\ 0 & \text{for } p \neq q. \end{cases} \quad (36)$$

The remaining four generic integrals $\int \varphi_p'(r) \varphi_q(r) dr$, $\int \varphi_p''(r) \varphi_q(r) dr$, $\int \varphi_p'(r) \varphi_q'(r) dr$ and $\int \varphi_p''(r) \varphi_q''(r) dr$ can be worked out in closed form. A generalized form of the solutions is also given by Ashton [22].

3. EXPERIMENTAL MEASUREMENTS AND DISCUSSIONS

In order to assess the modal damping arising from the material itself, extraneous sources of damping must be kept to the minimum possible. For that reason, many qualitative modal damping tests are performed on beams or plates which are essentially free–free. Furthermore, since a free edge is the most readily realizable of boundary conditions, tests on free–free specimens can be expected to produce a closer correlation between the experimental and theoretical data.

In the present work, the plate was supported with all the edges free. This was achieved by suspending the plate by light cotton threads from two points on the edge(s) coinciding with nodal points in that particular mode. The plate was subsequently subjected to excitation using a loudspeaker. The latter was held facing the plate at a reasonably short distance. A laser vibrometer was used as the means for non-contacting vibration pick up. For each mode, having verified that the nodal lines corresponded with the predicted nodal pattern, the SDC was then measured from the free decay of the resonant vibration.

Modal test results were obtained for a number of rectangular, mid-plane symmetric CFRP-laminated plates made from two different fibre materials. Several basic lay-ups were considered, including the zero-degree uni-directional and cross-ply laminates, a planar isotropic laminate and a thicker laminate consisting of +45, –45 and 0° layers. The first two laminates are specially orthotropic and show no bending–twisting coupling effect ($D_{16} = D_{26} = 0$), whereas the last two lay-ups are anisotropic and induce bending–twisting coupling, much more so in the case of the $\pm 45/0^\circ$ laminate. The orthotropic mechanical and damping properties of each material were measured using dynamic tests on uni-directional beam specimens, as described by Adams and Maheri [8]. The CFRP material data are listed in Table 1.

Figure 2 shows the convergence of the Rayleigh–Ritz solutions for the frequency and SDC in the fundamental mode, as the total number of the terms, M and N , in the assumed

TABLE 1

Orthotropic elastic and damping properties of CFRP materials

Material	E_1 (GPa)	E_2 (GPa)	G_{12} (GPa)	ν_{12}	ψ_1 (%)	ψ_2 (%)	ψ_{12} (%)	ρ (kg/m ³)
913C-HTA	124.5	10.2	6.3	0.34	0.55	4.98	5.92	1532
913C-TS [†]	110.0	9.0	3.9	0.34	0.75	5.95	6.79	1513

[†]Experimental data from reference [9].

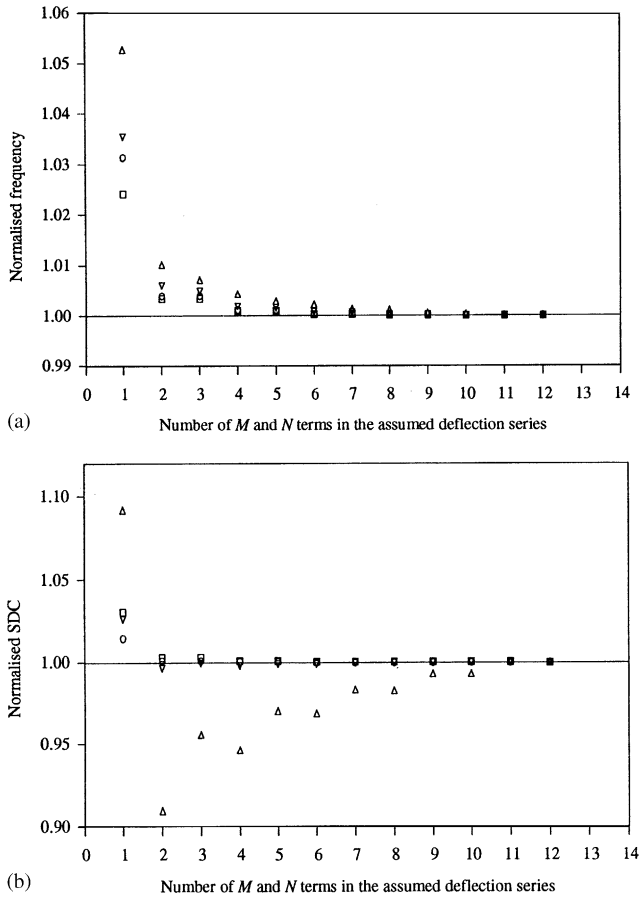


Figure 2. Convergence of the solution for (a) frequency and (b) SDC in the fundamental mode of various laminates (O, all-zero; □, cross-ply; ▽, planar isotropic; △, ±45/0).

deflection series (equation (22)) are increased. The frequency and SDC values in this figure have been normalized with respect to the values obtained from the last solution shown in each case ($M = N = 12$). In the case of the specially orthotropic laminates, as well as the planar-isotropic laminate, the solutions for both the frequency and SDC are seen to be already well converged by the time of using a (6 × 6) term solution. The remaining plate, the ±45/0 laminate, is highly anisotropic. As the figure indicates, the more anisotropic the laminate is, the slower is the convergence of the solution [13, 18]. This is particularly so in the case of the SDC value (Figure 2(b)), which is a function of the mode shape. Slow

TABLE 2

All-zero unidirectional 913C-TS plate ($a = 252$ (mm), $b = 192$ (mm), $h = 1.155$ (mm))

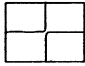
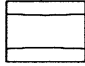
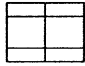
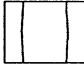
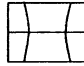
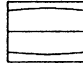
							
Freq. (Hz)	RR	41.0	78.4	114.53	160.0	179.2	217.4
	FE	41.0	83.4	118.0	161.6	180.3	234.6
	Exp.	39.2	76.4	111.8	161.9	178.6	215.5
SDC (%)	RR	6.69	5.94	6.31	0.76	2.06	5.88
	FE	6.70	5.93	6.28	0.78	2.07	5.85
	Exp.	8.33	5.36	7.13	0.67	2.31	5.51

TABLE 3

Cross-ply (0,90,0,90) s 913C-HTA plate ($a = 289$ (mm), $b = 287$ (mm), $h = 1.050$ (mm))

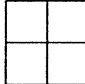
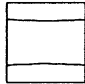
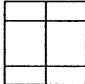
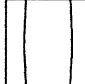
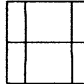
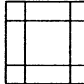
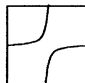
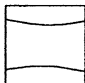
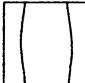


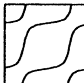
							
Freq. (Hz)	RR	27.6	71.9	91.1	98.9	113.2	167.0
	FE	27.6	72.2	91.3	101.6	115.5	169.8
	Exp.	28.6	69.6	88.3	97.4	111.1	149.4
SDC (%)	RR	5.74	1.21	2.90	0.71	1.89	3.08
	FE	5.75	1.25	2.92	0.73	1.85	3.06
	Exp.	5.73	1.47	3.69	0.64	1.87	4.40

TABLE 4

Planar-isotropic (0, 90, 45, -45) s 913C-HTA plate ($a = 287$ (mm), $b = 287$ (mm), $h = 1.045$ (mm))

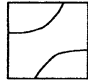
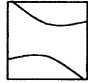
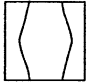
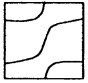
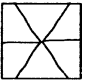
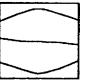
							
Freq. (Hz)	RR	33.4	73.0	95.2	98.5	117.4	181.4
	FE	33.4	74.0	96.7	99.5	118.1	183.8
	Exp.	38.5	71.4	94.5	101.5	120.2	180.9
SDC (%)	RR	3.72	1.20	0.80	2.40	1.73	2.49
	FE	3.73	1.23	0.84	2.41	1.73	2.53
	Exp.	3.18	1.42	0.91	2.66	1.93	2.80

convergence is attributed to the skewness of nodal patterns, and this is a characteristic of the anisotropic plates.

The modal data of the free-free plates are tabulated in Tables 2–5 for the first six modes in ascending order of the frequency. The data include the theoretical values of modal

TABLE 5

The (45, -45, 0, 0, 0, 45, -45, 0, 0) s 913C-TS plate ($a = 254$ (mm), $b = 254$ (mm), $h = 2.320$ (mm))

							
Freq. (Hz)	RR	128.3	139.1	245.7	301.7	341.3	425.9
	FE	128.1	138.7	246.6	300.0	337.1	435.7
	Exp.	135.3	146.8	237.3	316.1	347.6	—
SDC (%)	RR	1.98	2.37	1.18	1.79	1.83	2.10
	FE	1.99	2.53	1.26	1.86	1.89	2.28
	Exp.	2.00	2.14	1.28	1.79	1.82	—

frequency and specific damping capacity obtained by the Rayleigh–Ritz method. A (6×6) term solution was used for all the laminates, except for the $\pm 45/0$ laminate, where a (12×12) term solution was used to ensure of full convergence. The theoretical nodal pattern of each mode is also shown (the plate and fibre co-ordinates are as specified in Figure 1). The experimental values (Exp.) are also listed.

The results obtained by the FE method are also listed in these tables for comparison. These latter values were obtained by using a FE analysis described by Lin *et al.* [5]. The analysis allows for transverse shear deformation by using a first order shear deformation theory, in a manner similar to that for a Mindlin-type plate. A parabolic distribution of shear stress over the cross-section is assumed. A (6×6) elements mesh was found to be adequate in the FE solutions.

As the tables show, the theoretical and experimental values correlate quite well. While in most cases these values are within only a few percent from one another, the largest difference between any one of the two sets of the theoretical and experimental data lies roughly in the range $\pm 13\%$ for the frequency, and in the range $+18$ to -30% for the damping values. Comparison of the Rayleigh–Ritz theoretical values with the FE predictions will show an even smaller difference in the frequency values, ranging from $+1$, to -7% , and in the damping values, ranging from $+2$ to -8% . It is evident, therefore, that not only does the Rayleigh–Ritz method predict reasonably accurately the experimental data, it also essentially reproduces the results of the FE method.

This is of particular interest in the light of the computational efficiency of the Rayleigh–Ritz method. In the present work, for example, using a (6×6) term solution, computation of the modal properties of the first six modes of the FRP-laminated plates, including the frequency, SDC and nodal patterns, took about 1 s on a medium-size desktop computer (about 10 s for the (12×12) term solution of the $\pm 45/0$ laminate).

The variation of modal damping with fibre orientations and the nodal patterns have been discussed by, for example, Lin *et al.* [5] and Maheri and Adams [9]. Some of the more important characteristics of modal damping are outlined here with reference to the present results. First, it is noted that when the bending axis is lateral to the lay of the fibres, the latter become highly stressed, and the elastic energy becomes relatively high, as a consequence of which, the modal SDC becomes relatively low. Conversely, when the bending axis becomes parallel to the lay of the fibres, little stress is borne by the fibres, and the elastic energy is relatively low and, as a result, the SDC becomes relatively high. This simple mechanism is clearly shown by comparing the 0–2 and 2–0 beam-type modes of the

all-zero uni-directional plate (Table 2, second and fourth modes respectively). The combined effect of fibre orientation and stacking sequence of the layers is demonstrated by comparing the 0–2 and the 2–0 modes of the cross-ply plate (Table 3, second and fourth modes respectively). The SDC of the 0–2 mode is more than twice that of the 2–0 mode. This is due to the fact that in the 0–2 mode, the stacking sequence number of the layers whose fibre lay is lateral to the bending axis is one above the stacking sequence number of the layers whose fibre lay is parallel to the bending axis, whereas in the 2–0 mode the situation is reversed. As a consequence, the bending stiffness of the 0–2 mode becomes lower than that of the 2–0 mode, and its SDC becomes higher. A similar situation can also be observed by comparing the beam-type modes of the planar–isotropic plate (Table 4, second and third modes). The results in Table 3 also demonstrate the significance of a twisting-type deformation in modal damping. This type of deformation is predominant when nodal lines cross one another, in which case the polymeric matrix in a FRP material experiences intense shearing. These modes are significantly more damped.

4. CONCLUSIONS

The theoretical modal damping of layered anisotropic plates can be readily estimated using basic laminated plate theory and a simple numerical method such as the Rayleigh–Ritz energy minimization scheme. The theoretical results were shown to correlate well with experimental data obtained for freely held plates, and to be at least as accurate as those obtained by the finite element method. The basic mechanisms governing the modal damping in laminated plates were highlighted, and these were shown to follow accurately the variation in such parameters as fibre orientation, stacking sequence and the nature of deformation in a particular mode of vibration.

REFERENCES

1. B. J. LAZAN 1968 *Damping of Materials and Members in Structural Mechanics*. London: Pergamon Press.
2. D. J. MEAD 1999 *Passive Vibration Control*. Chichester, U.K.: John Wiley & Sons Ltd.
3. R. D. ADAMS and D. G. C. BACON 1973 *Journal of Composite Materials* **7**, 402–428. Effect of fibre orientation and laminate geometry on the dynamic properties of CFRP.
4. R. G. NI and R. D. ADAMS 1984 *Journal of Composite Materials* **18**, 104–121. The damping and dynamic moduli of symmetric laminated composite beams—theoretical and experimental results.
5. D. X. LIN, R. G. NI and R. D. ADAMS 1984 *Journal of Composite Materials* **18**, 132–152. Prediction and measurement of the vibrational damping parameters of carbon and glass fibre-reinforced plastics plates.
6. R. D. ADAMS and R. F. LAMBERT 1986 *Vibration Damping Workshop II, Las Vegas, Nevada*, AFWAL-TR-863059. A design methodology for estimating the damping in laminated and fibre-reinforced plates.
7. N. ZABARA and T. PERVEZ 1990 *Computer Methods in Applied Mechanics and Engineering* **81**, 291–316. Viscous damping approximation of laminated anisotropic composite plates using the finite element method.
8. R. D. ADAMS and M. R. MAHERI 1994 *Composite Science and Technology* **50**, 497–514. Dynamic flexural properties of anisotropic fibrous composite beams.
9. M. R. MAHERI and R. D. ADAMS 1995 *Composite Science and Technology* **55**, 13–23. Finite-element prediction of modal response of damped layered composite panels.
10. J. H. YIM and J. W. GILLESPIE Jr 2000 *Composite Structures* **50**, 217–225. Damping characteristics of 0 and 90 of AS4/3501-6 unidirectional laminates including the transverse shear effect.

11. D. A. SARAVANOS and C. C. CHAMIS 1990 *Polymer Composites* **11**, 328–336. An integrated methodology for optimizing the passive damping of composite structures.
12. D. A. SARAVANOS and C. C. CHAMIS 1991 *NASA Technical Memorandum* 104497. The effects of interply damping layers on the dynamic response of composite structures.
13. J. E. ASHTON and J. M. WHITNEY 1970 *Theory of Laminated Plates*. CT, U.S.A.: Technomic Publishing Company.
14. J. E. ASHTON and M. E. WADDUPS 1969 *Journal of Composite Materials* **3**, 148–165. Analysis of anisotropic plates.
15. L. R. DEOBALD and R. F. GIBSON 1988 *Journal of Sound and Vibration* **124**, 269–283. Determination of elastic constants of orthotropic plates by a modal analysis/Rayleigh–Ritz technique.
16. D. YOUNG 1950 *Journal of Applied Mechanics* **17**, 448–453. Vibration of rectangular plates by the Ritz method.
17. D. J. DAWE and O. L. ROUFAEIL 1980 *Journal of Sound and Vibration* **69**, 345–359. Rayleigh–Ritz vibration analysis of mindlin plates.
18. T. J. CRAIGE and D. J. DAWE 1986 *International Journal of Solids and Structures* **22**, 155–169. Flexural vibration of symmetrically laminated composite rectangular plates including transverse shear effects.
19. R. B. BAHT 1984 *Journal of Sound and Vibration* **102**, 493–499. Natural frequencies of rectangular plates using characteristic orthogonal-polynomials in Rayleigh–Ritz method.
20. C. RAJALINGHAM, R. B. BAHT and G. D. XISTRIS 1996 *Journal of Sound and Vibration* **193**, 497–509. Vibration of rectangular plates using plate characteristic functions as shape functions in the Rayleigh–Ritz method.
21. O. C. ZIENKIEWICZ and R. L. TAYLOR 1991 *The Finite Element Method*, Vol. 2. London, U.K.: McGraw-Hill International (U.K.) Ltd.
22. J. E. ASHTON 1969 *Journal of Composite Materials* **3**, 470–479. Analysis of anisotropic plates II.